OPEN ACCESS Freely available online

PLOS ONE

^{11}C-Acetate PET Imaging in Patients with Multiple Sclerosis

Kazushiro Takata[1☯], Hiroki Kato[2☯], Eku Shimosegawa[2], Tatsusada Okuno[1], Toru Koda[1], Tomoyuki Sugimoto[3], Hideki Mochizuki[1], Jun Hatazawa[2,4*], Yuji Nakatsuji[1*]

1 Department of Neurology, Osaka University Graduate School of Medicine, Suita, Osaka, Japan, **2** Department of Nuclear Medicine and Tracer Kinetics, Osaka University Graduate School of Medicine, Suita, Osaka, Japan, **3** Hirosaki University Graduate School of Science and Technology, Hirosaki, Aomori, Japan, **4** WPI-Immunology Frontier Research Center, Osaka University, Suita, Osaka, Japan

Abstract

Background: Activation of glial cells is a cardinal feature in multiple sclerosis (MS) pathology, and acetate has been reported to be selectively uptaken by astrocytes in the CNS. The aim of this study was to investigate the efficacy of PET with ^{11}C-acetate for MS diagnosis.

Materials and Methods: Six patients with relapsing-remitting MS and 6 healthy volunteers (HV) were enrolled. The ^{11}C-acetate brain uptake on PET was measured in patients with MS and HV. Volume-of-interest analysis of cerebral gray and white matter based on the segmentation technique for co-registered MRI and voxel-based statistical parametric analysis were performed. Correlation between ^{11}C-acetate uptake and the lesion number in T1- and T2- weighted MR images were also assessed.

Results: The standardized uptake value (SUV) of ^{11}C-acetate was increased in both white and gray matter in MS patients compared to HV. Voxel-based statistical analysis revealed a significantly increased SUV relative to that in the bilateral thalami (SUVt) in a broad area of white matter, particularly in the subcortical white matter of MS patients. The numbers of T2 lesions and T1 black holes were significantly correlated with SUV of ^{11}C-acetate in white and gray matter.

Conclusions: The ^{11}C-acetate uptake significantly increased in MS patients and correlated to the number of MRI lesions. These preliminary data suggest that ^{11}C-acetate PET can be a useful clinical examination for MS patients.

Citation: Takata K, Kato H, Shimosegawa E, Okuno T, Koda T, et al. (2014) ^{11}C-Acetate PET Imaging in Patients with Multiple Sclerosis. PLoS ONE 9(11): e111598. doi:10.1371/journal.pone.0111598

Editor: Akio Suzumura, Research Inst. of Environmental Med., Nagoya Univ., Japan

Received August 21, 2014; **Accepted** September 25, 2014; **Published** November 4, 2014

Data Availability: The authors confirm that all data underlying the findings are fully available without restriction. All relevant data are within the paper and its Supporting Information files.

Funding: This study was supported by the Health and Labor Sciences Research Grants from the Ministry of Health, Labor and Welfare of Japan, by a Grant-in-Aid for Scientific Research of Japan Society for the Promotion of Science (YN and TO) and by the Japan Society for the Promotion of Science KAKENHI Grant Number 23592089 (HK). The funders had no role in study design, data collection and analysis, decision to publish, or preparation of the manuscript.

Competing Interests: The authors have declared that no competing interests exist.

* Email: hatazawa@tracer.med.osaka-u.ac.jp (JH); yuji@neurol.med.osaka-u.ac.jp (YN)

☯ These authors contributed equally to this work.

Introduction

Multiple sclerosis (MS) is an inflammatory demyelinating autoimmune disease of the CNS [1]. Although MRI is recognized as the most informative surrogate marker [2], the diagnostic value of MRI in MS remains insufficient [3]. Glial activation is a key feature in the neuroinflammatory MS pathology, and glial activation from the early phase of MS is suggested by a MRS study [4]. Microglial activation has also been shown in PET studies [5,6]. However, astrocyte activation in MS has not been evaluated in vivo due to the lack of an appropriate radioligand, despite the astrocytosis observed from the early phase of disease and the important role potentially played by astrocytes [4,7,8].

Acetate is converted into fatty acids by the key enzyme acetyl-CoA synthase and metabolized in the citric acid cycle. ^{11}C-acetate has been used as a tracer to evaluate cardiac oxidative metabolism [9] and later used as a PET biomarker in patients with renal cell carcinoma, hepatocellular carcinoma, prostate cancer, and multiple myeloma [10,11,12,13]. In the CNS, ^{11}C-acetate PET has proven useful for the diagnosis of astrocytoma [14] because acetate is preferentially absorbed into astrocytes by the monocarboxylate transporter (MCT) [15,16]. Notably, the expression of MCT is increased in MS brains [17]. Therefore, we surmised that ^{11}C-acetate PET could be a useful diagnostic tool in combination with MRI, and we investigated the utility of ^{11}C-acetate PET for the diagnosis of MS and evaluated the astrocyte activity in the MS brain.

Materials and Methods

Subjects and clinical evaluation

Six patients with relapsing-remitting MS were evaluated. All patients were in the remission phase. Disability was assessed based

Table 1. Patient data and demographics.

	sex	age	type	therapy	EDSS score	Disease duration (y)	GM SUVt	WM SUVt	WM/GM ratio
MS 1	F	47	RR	IFNβ, MTX	7	10.3	1.0494	0.9415	0.8972
MS 2	F	45	RR	IFNβ	2	6.8	1.1069	1.0529	0.9512
MS 3	F	48	RR	IFNβ	1	5.7	1.0282	0.8874	0.8631
MS 4	F	53	RR	IFNβ	2.5	7.4	1.0837	0.9434	0.8705
MS 5	F	34	RR	-	4	3.3	0.9633	0.8244	0.8558
MS 6	F	49	RR	-	1	1.4	1.0336	0.9044	0.8750
HV 1	F	54					0.9149	0.7320	0.8001
HV 2	F	61					0.9671	0.8121	0.8397
HV 3	F	41					0.9518	0.7789	0.8183
HV 4	F	67					0.9341	0.7946	0.8507
HV 5	F	62					0.9449	0.8021	0.8489
HV 6	F	63					0.9758	0.8096	0.8297

MS = multiple sclerosis, HV = healthy volunteer, RR = relapsing-remitting multiple sclerosis, IFNβ = interferon beta treatment, MTX = Mitoxantrone, EDSS = Expanded Disability Status Scale, SUV = standardized uptake value.

doi:10.1371/journal.pone.0111598.t001

on the Expanded Disability Status Scale (EDSS) [18]. Six healthy volunteers (HV) served as normal controls (Table 1). This study was approved by the Ethics Committee of Osaka University Hospital, and written informed consent was obtained from each participant.

MRI

MRI was performed using a GE SIGNA HDxt 3.0-T or a Phillips Achieva 3.0-T scanner. Three-dimensional (3D) structural MRI was performed for each subject using a T1-weighted spoiled gradient recalled (SPGR) sequence (axial plane; slice thickness, 0.90/0.95 mm; matrix size, 512×512; in-plane resolution, 0.47×0.47 mm; TR, 2.144 to 2.192/2.477 to 2.53 ms; TE, 6.908 to 7.108/6.000; flip angle, 18°/15°) and T2-weighted two-dimensional fast spin echo sequences (axial plane; FOV 250 mm; matrix size, 512×512; slice thickness, 5 mm; interslice gap, 1 to 1.5 mm; TE, 89/80 ms; TR, 4500/3000 ms).

PET

PET was performed using a SET-3000 GCT/X scanner (Shimadzu Corp., Kyoto, Japan). ^{11}C-acetate was synthesized by carbonation of Grignard reagent followed by acid hydrolysis. ^{11}C-carbon dioxide reacted with methylmagnesium bromide followed by hydrolysis with hydrochloric acid to yield ^{11}C acetic acid [19]. The radio chemical purity was greater than 98%. A total of 370 MBq of the tracer was administered intravenously, and a 20-min emission acquisition was initiated 20 min later. PET images were obtained in a 3-D mode. The images were reconstructed using a filtered-back projection method after 3D Gaussian smoothing with a 6-mm full width at half maximum (FWHM). Scatter correction was performed using a hybrid dual-energy window method combined with a convolution-subtraction method, and the true scatter-free component of the standard photopeak window was estimated sonographically. All PET images were reconstructed in 256×256×99 anisotropic voxels, with each voxel measuring 1×1×2.6 mm.

Data analysis

Whole brain VOI analysis. All procedures were performed using a personal computer (DELL Precision T7400; DELL Inc., Round Rock, TX, USA) running on Microsoft Windows 7 (Microsoft Corp., Redmond, WA, USA). The 3D T1-weighted MRI scan was re-sliced in the native space of each subject using a 1.0×1.0×1.0 mm voxel size. The results were first categorized as GM, WM, and CSF, then spatially normalized using the unified model [20] of Statistical Parametric Mapping (SPM) 8 (Wellcome Department of Imaging Neuroscience: http://www.fil.ion.ucl.ac.uk/spm/) according to the optimized voxel-based morphometry (VBM) protocol [21]. This generated both spatial normalization matrices and inverse spatial normalization matrices. The resulting normalized GM map was transformed into native space using an inverse spatial normalization matrix. To generate VOI for GM and/or WM, binary mask images for the GM and/or WM were created using the segmented images in the native space of each subject. The binary mask image boundary was set at 35% of the maximum GM or WM concentration as described in previous studies [22,23].

The ^{11}C-acetate PET images were co-registered with the resliced 3D T1-weighted MRI using the SPM8 registration function based on the mutual information. The co-registration precision was inspected with the "Check Registration" tool in SPM8. Then, the co-registered PET images were spatially transformed using normalization and/or inverse normalization matrices identical to those generated in the previously described

automatic segmentation process. The ^{11}C -acetate uptake in the GM and WM VOI was analyzed using the binary masks within the native space.

To minimize contamination from the spill-in effect of adjacent brain segments, the spill-in-free VOIs of GM and WM were generated by the VOI erosion process. First, the binary masks were blurred by convolution using the point spread function of the PET scanner (presumably a simple isotropic Gaussian kernel with a FWHM of 8 mm). The spill-in-free gray matter mask $\hat{G}$ is expressed as follows:

$$\hat{G} = \{x \in G | \tilde{W}(x) < 0.1\},$$

where x is a voxel, G is the gray matter binary mask, and $\tilde{W}(x)$ is the blurred image of the white matter binary mask (i.e. spill-in fraction from the white matter to the voxel x). The spill-in-free white matter mask was also constructed as described above. Spill-in from CSF was assumed as zero. VOI analysis for ^{11}C-acetate uptake using spill-in-free GM and WM masks was also performed (Figure S1).

The relative standardized uptake value (SUVt) served as the uptake indicator for analysis; the regional standardized uptake value (SUV) was divided by the mean SUV within the bilateral thalami of each subject. The Mann–Whitney U test was performed to determine significance of ^{11}C -acetate SUVt differences between MS and HV. The significance level was designated at $p<0.05$.

Voxel-based statistical analysis. Voxel-based whole brain SUVt in the MS and HV groups was compared using Statistical Parametric Mapping (SPM) 8 (Wellcome Department of Imaging Neuroscience). The spatially normalized PET images were smoothed using a 12-mm FWHM isotropic Gaussian kernel, which conditions the residuals to conform more closely to the Gaussian random field model underlying the statistical adjustment of the p values. The SPM statistical model used voxel-by-voxel "two-sample T-test with covariates," which designated age as a nuisance variable in order to detect voxels showing a significant age-adjusted SUVt difference between the MS and HV groups.

11C-acetate uptake and the MR images correlation assessment. The T2 and T1 black hole lesions were independently recorded visually by three observers. T1 black holes were defined as visible hypointense regions on the T1- weighted images coincident with a high signal intense region on the T2-weighted images. Each MRI mask image was divided into its hemispheres to create the hemispheric VOIs. Pearson product moment correlation analyses were performed to assess the association between the number of MRI lesions, and the SUV of ^{11}C-acetate was accessed from the hemispheric VOIs of the GM and WM. Statistical significance was designated at $p<0.05$.

Statistical analysis

The data in Fig 1 and Table S1 were analyzed using the Mann–Whitney U test. ANCOVA was used to assess the differences between age-adjusted groups illustrated in Fig 2B–G, and Pearson product moment correlation analyses were performed for data in Fig 3, SPSS 14.J was used for statistical analysis.

Results

VOI analysis of the ^{11}C-acetate SUV revealed that the mean SUV was higher in the MS patients than in the HV in all regions assessed (Fig 1A). To evaluate the regional distribution of ^{11}C-acetate uptake independent of physiologic variation in the whole brain, we calculated the relative uptake value (SUVt), which is the regional SUV divided by the mean SUV within the bilateral thalami of each participant (Fig 1B). The thalamus served as the reference region because it is rarely involved in MS pathology [24], and the SUV difference between the thalamus of HV and MS patients was the least among brain regions, as shown in Fig 1A. Each regional SUVt in the MS patients were increased particularly in the parietal, occipital, and insula regions.

Spatially normalized group mean images of ^{11}C-acetate SUVt automatically segmented based on MRI showed increased uptake in both WM and GM in MS patients (Fig 2A). The SUVt of MS patients was significantly higher than that of HV in both WM ($p = 0.002$) and GM ($p = 0.001$). In addition, all six MS patients had a significantly higher WM/GM SUV ratio than the six HV ($p = 0.009$) (Fig 2B–D). This trend was consistently observed even after accommodating spill-in effect from adjacent brain segments (Fig 2E–G). Collectively, the ^{11}C-acetate uptake significantly increased in both the WM and GM of MS patients, and this increase was more predominant in WM. The whole brain SPM analysis revealed a significant increase in SUVt of voxel cluster in MS patients compared to HV, primarily in the subcortical frontal, parietal, and occipital regions; no voxels showed a significantly lower SUVt in MS patients compared to HV (Fig 2H).

The voxel-based t-statistic for the WM tracts showed a significantly increased mean T-score, predominantly in the superior longitudinal fasciculus, posterior thalamic radiation, and sagittal stratum, with the highest local maximum T-score in the corpus callosum (Table S2).

We then assessed potential correlation between ^{11}C-acetate SUV and MRI brain lesions. The mean SUV in WM was significantly correlated to the number of T1 black holes ($R^2 = 0.5059$, $p = 0.009$) and T2 lesions ($R^2 = 0.4594$, $p = 0.015$) (Fig 3A, B). The mean SUV in GM also correlated to the number of T1 black holes ($R^2 = 0.4088$, $p = 0.025$) and T2 lesions ($R^2 = 0.3952$, $p = 0.029$) (Fig 3C, D). The correlation to the EDSS score and disease duration did not reach statistical significance.

Discussion

There have been few studies imaging astrocytes in vivo using ^{11}C-acetate PET. In MS, astrocyte proliferation [25] and formation of scars composing a dense network of hypertrophic cells are characteristics of the MS histopathology [8]. An increased MCT expression in astrocytes within MS lesions was recently shown by immunohistochemical analysis [17], which suggest an increase in astrocyte metabolism. However, latent autoantibody-mediated astrocyte damage [26] supposedly decreases the metabolic activity, and therefore, the metabolic activity of astrocytes in MS brains remains undetermined. In this study, we observed a significantly increased brain uptake of the radioligand ^{11}C-acetate in MS patients. Our study revealed for the first time that astrocytes are generally activated in MS brains based on the acetate metabolism.

Representative studies showed that a higher value in the kinetic parameter, which indicates the washout level of ^{11}C-acetate, reflects the astrocyte reactivity in normal rats and healthy humans [27]. In MS, however, compared to HV, the pathologic changes in the severity of ^{11}C-acetate accumulation may be much more prominent than the changes related to physiologic activation in healthy humans. Therefore, a slight increase in the washout speed may be inapparent in the PET SUV in MS. Furthermore, because the perfusion in the normal appearing white matter decreased in MS [28], the increase in ^{11}C-acetate uptake by static PET may be underestimated due to a reduced CBF in MS.

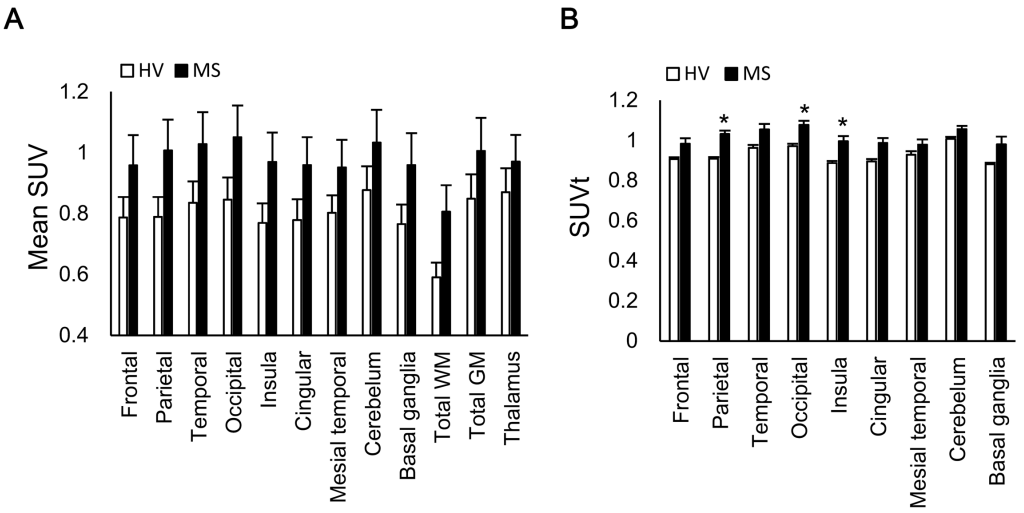

Figure 1. ^{11}C-acetate CNS biodistribution. (A)Mean standardized uptake value (SUV) of each lesion. (B) Relative SUV compared to that of the thalamus (SUVt). Data are expressed as the mean ± standard error of the mean (SEM) (n = 6). The Mann–Whitney *U* test showed a significant difference in the median between the HV and MS groups (*:p<0.0055 after Bonferroni correction). HV = healthy volunteers, MS = multiple sclerosis.
doi:10.1371/journal.pone.0111598.g001

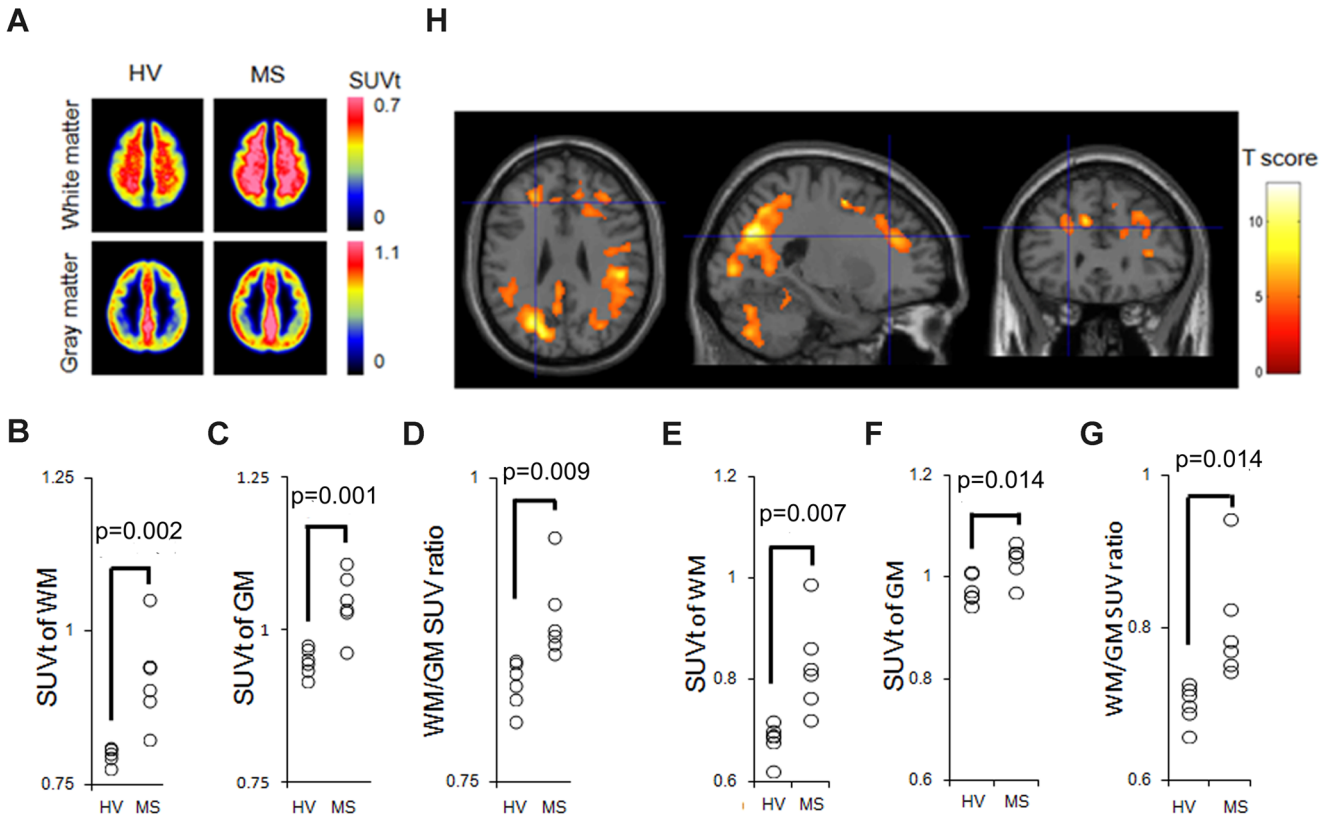

Figure 2. ^{11}C-acetate uptake distribution and quantification in MS patients. (A)Spatially normalized group mean images of ^{11}C-acetate SUVt automatically segmented based on MRI. VOI analysis summarizing the mean SUVt in WM (B) and GM (C), and the WM/GM SUV ratio (D) in the HV and MS groups. The identical analysis performed using spill-in-free VOIs are also shown (E–G). The p-value was calculated using the analysis of covariance to adjust the variance of age. (H) The SPM analysis result is overlaid onto the T1-weighted brain MRI template. Colored voxels indicate T-scores representing significantly increased ^{11}C-acetate uptake (SUVt) in patients with MS compared to HV patients. The spatially normalized PET images were smoothed for the analysis using a 12-mm FWHM isotropic Gaussian kernel. The significance thresholds are corrected for multiple comparisons at the cluster level with a p-value of 0.05 (family-wise error correction). SUV: standardized uptake value.
doi:10.1371/journal.pone.0111598.g002

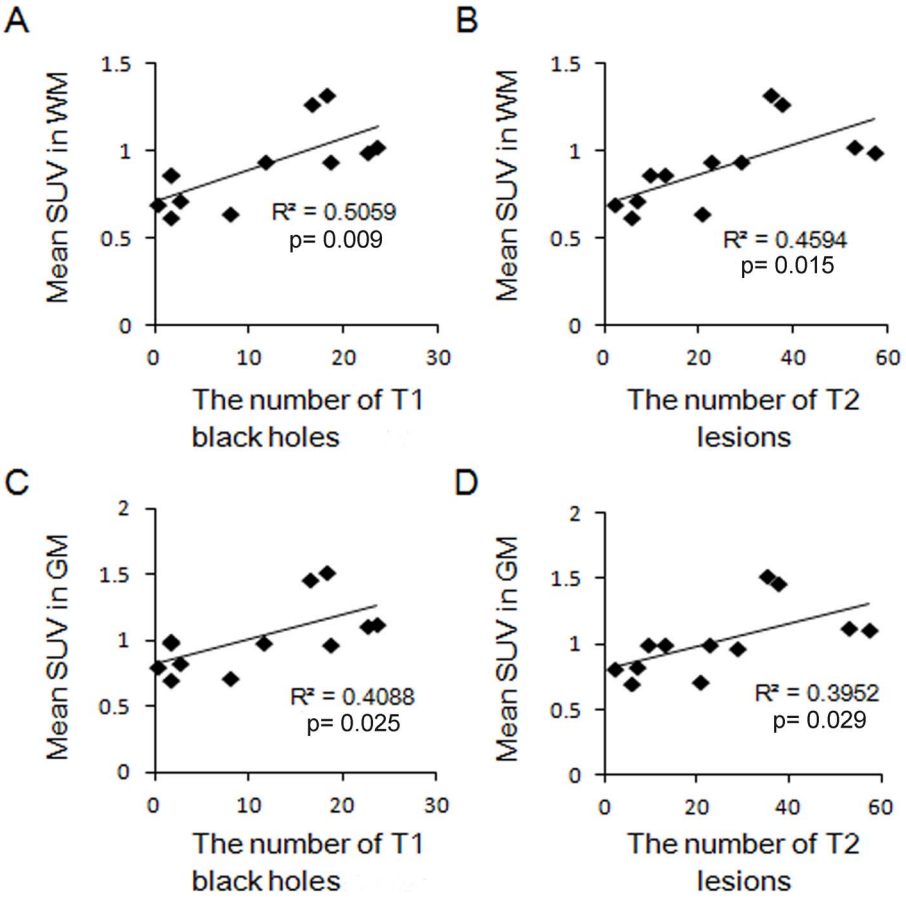

Figure 3. Correlation between ^{11}C-acetate SUV and the number of MRI lesions in patients with MS. Correlation between ^{11}C-acetate SUV in WM or GM and the number of T1 black holes (A, C) or T2 lesions (B, D) in each hemisphere of the six MS patients. SUV: standardized uptake value.
doi:10.1371/journal.pone.0111598.g003

The increased uptake was more pronounced in the WM, although a significant increase was observed in both the WM and GM. A significantly increased uptake was observed primarily within the subcortical WM on the voxel-based statistical analysis (Fig. 2H). On the voxel-based statistical analysis of the WM tracts, the distribution of the increased acetate uptake was similar to that in regions of axonal damage in DTI studies (Table S2). Recent voxel- and tract-based analyses in DTI studies revealed widespread damage to the subcortical WM, particularly in the sagittal stratum, corpus callosum, posterior thalamic radiation, and corona radiata [29]. These data suggested that the region-dependent increased acetate uptake was induced by the reactive astrocyte coexisting with heterogeneously dispersed MS lesions detected in DTI studies (Fig. 2H and Table S2). Although inflammatory WM demyelination detected by conventional MRI is a cardinal feature of MS, pathologic changes exist even in normal appearing WM and GM [30]. Astrocyte pathology precedes demyelination in an animal model [31]; astrocyte hypertrophy occurs at the leading edge of acute MS lesions, followed later by astrocytic scarring [8]. Thus, the altered astrocyte activation is presumably involved in MS pathophysiology [4,7,32]. Correlation between the radial diffusivity quantified by DTI and T1 black hole formation are recognized markers of axonal loss and tissue destruction [33,34]. In the present study, the strongest correlation was detected between the mean SUV in WM and the T1 black hole number, suggesting that the mean SUV may correlate with axonal damage. The mean SUV in GM also increased and correlated with the number of MRI lesions, suggesting cortical astrocyte involvement in MS pathology. Cortical involvement and subsequent cognitive decline occur in approximately half of MS patients [35]. However, little information exists on the pathophysiologic involvement of cortical astrocytes [36]. Normally, astrocytes supply lactate to neurons for oxidation [37], and metabolic dysfunction of neurons and glial cell activation likely occurs in the MS brain [25]. Moreover, astrocytes are associated with preclinical axonal damage in an animal model of MS [38]. These results suggest that the increased ^{11}C-acetate uptake within GM may reflect astrocyte-associated cortical damage in MS.

The present study has a few limitations. First, ^{11}C-acetate uptake in MS plaques was not assessed separately because most plaques were so small that a partial volume effect caused by the relatively low resolution of PET was inevitable. Second, the analysis was performed on static PET data instead of kinetic parameters. In the present study, the data acquired between 20 to 40 min after tracer administration were summed to build static uptake images because the time activity curve stabilized after 20 min (data not shown). Regional uptake distribution may be contaminated by the dispersion of radioactive metabolites. However, in our study, 1-^{11}C-acetate was used, and its dispersion of labeled metabolites was the smallest among the various types of acetate tracers [39,40]. In addition, because almost all the tracer was first absorbed through MCT-1 expressed within astrocytes according to their reactivity, the summed radioactivity is thought to reflect the first uptake of ^{11}C- acetate and its subsequent

metabolism by reactive astrocytes. Finally, because the mean age was higher in the control group than in the MS group, we used the ANCOVA to assess the differences among the age-adjusted SUVt. Although the mean age of MS patients was generally lower than that of the healthy volunteers, age did not significantly affect the increased uptake of ^{11}C-acetate in MS patients.

Conclusions

The present study suggests that the pathologic white matter changes in patients with MS can be detected by non-invasive static ^{11}C-acetate PET, which may be an effective MS diagnostic tool. Development of clinically applicable monocarbonic acid tracers labeled with longer half-life radioactive nuclides are needed, as are further studies enrolling more participants, including those in the early and relapse phases.

Supporting Information

Figure S1 Binary mask imaging parameters for VOI analysis. The scheme of VOI analysis is described. A: ^{11}C-acetate PET, B: 3D MRI, C: Co-registration, D: Spatial normalization to the MNI space, E/F: Segmented GM/WM map in the MNI space, G/H: GM/WM binarized mask in the original space of the subject, I/J: Eroded version of G/H for spill-in-free VOI analysis, K–N: GM/WM masks overlaid onto PET in the original space of the subject. MNI: montreal neurological institute. f: Transformation matrix for spatial normalization, f^{-1}: Inverse of the transformation.
(TIF)

Table S1 Relative ^{11}C-acetate biodistribution in the CNS. The mean SUVt of each lesion in the CNS was analyzed and for group comparison between HV and MS patients, the Mann–Whitney *U* test was performed.
(DOC)

Table S2 Regional T-scores from voxel-based statistical comparison in WM. Voxel-based statistical comparison in white matter tracts was performed. The positive T-scores indicate an increased ^{11}C-acetate uptake in the MS patients compared to the HV.
(DOC)

Text S1 Supplementary methods. Methods for "Voxel-based statistical analysis for WM tracts" are described with references.
(DOC)

Acknowledgments

We thank Dr. Hisashi Tanaka, Dr. Yoshiyuki Watanabe, Dr. Kayako Isohashi, Mr. Koichi Fujino, Mr. Yasukazu Kanai, Mr. Sadahiro Naka, and the staff of the Department of Nuclear Medicine and the Cyclotron staff of Osaka University Hospital for their technical support in performing the studies.

Author Contributions

Conceived and designed the experiments: YN HM JH. Performed the experiments: HK ES. Analyzed the data: KT HK TO TK TS. Wrote the paper: KT HK YN.

References

1. Compston A, Coles A (2002) Multiple sclerosis. Lancet 359: 1221–1231.
2. Sormani MP, Bruzzi P (2013) MRI lesions as a surrogate for relapses in multiple sclerosis: a meta-analysis of randomised trials. Lancet Neurol 12: 669–676.
3. Odenthal A, Coulthard C (2014) The Prognostic Utility of MRI in Clinically Isolated Syndrome: A Literature Review. AJNR Am J Neuroradiol.
4. Fernando KT, McLean MA, Chard DT, MacManus DG, Dalton CM, et al. (2004) Elevated white matter myo-inositol in clinically isolated syndromes suggestive of multiple sclerosis. Brain 127: 1361–1369.
5. Banati RB, Newcombe J, Gunn RN, Cagnin A, Turkheimer F, et al. (2000) The peripheral benzodiazepine binding site in the brain in multiple sclerosis: quantitative in vivo imaging of microglia as a measure of disease activity. Brain 123 (Pt 11): 2321–2337.
6. Politis M, Giannetti P, Su P, Turkheimer F, Keihaninejad S, et al. (2012) Increased PK11195 PET binding in the cortex of patients with MS correlates with disability. Neurology 79: 523–530.
7. Black JA, Newcombe J, Waxman SG (2010) Astrocytes within multiple sclerosis lesions upregulate sodium channel Nav1.5. Brain 133: 835–846.
8. Brosnan CF, Raine CS (2013) The astrocyte in multiple sclerosis revisited. Glia 61: 453–465.
9. Brown M, Marshall DR, Sobel BE, Bergmann SR (1987) Delineation of myocardial oxygen utilization with carbon-11-labeled acetate. Circulation 76: 687–696.
10. Oyama N, Okazawa H, Kusukawa N, Kaneda T, Miwa Y, et al. (2009) 11C-Acetate PET imaging for renal cell carcinoma. Eur J Nucl Med Mol Imaging 36: 422–427.
11. Ho CL, Yu SC, Yeung DW (2003) 11C-acetate PET imaging in hepatocellular carcinoma and other liver masses. J Nucl Med 44: 213–221.
12. Oyama N, Akino H, Kanamaru H, Suzuki Y, Muramoto S, et al. (2002) 11C-acetate PET imaging of prostate cancer. J Nucl Med 43: 181–186.
13. Lin C, Ho CL, Ng SH, Wang PN, Huang Y, et al. (2014) (11)C-acetate as a new biomarker for PET/CT in patients with multiple myeloma: initial staging and postinduction response assessment. Eur J Nucl Med Mol Imaging 41: 41–49.
14. Liu RS, Chang CP, Chu LS, Chu YK, Hsieh HJ, et al. (2006) PET imaging of brain astrocytoma with 1-11C-acetate. Eur J Nucl Med Mol Imaging 33: 420–427.
15. Waniewski RA, Martin DL (1998) Preferential utilization of acetate by astrocytes is attributable to transport. J Neurosci 18: 5225–5233.
16. Hosoi R, Okada M, Hatazawa J, Gee A, Inoue O (2004) Effect of astrocytic energy metabolism depressant on 14C-acetate uptake in intact rat brain. J Cereb Blood Flow Metab 24: 188–190.
17. Nijland PG, Michailidou I, Witte ME, Mizee MR, van der Pol SM, et al. (2014) Cellular distribution of glucose and monocarboxylate transporters in human brain white matter and multiple sclerosis lesions. Glia 62: 1125–1141.
18. Kurtzke JF (1983) Rating neurologic impairment in multiple sclerosis: an expanded disability status scale (EDSS). Neurology 33: 1444–1452.
19. Ishiwata K, Ishii S-I, Senda M (1995) Successive preparation of 11C labeled sodium acetate and/or sodium hexanoate. Applied Radiation and Isotopes 46: 1035–1037.
20. Ashburner J, Friston KJ (2005) Unified segmentation. Neuroimage 26: 839–851.
21. Good CD, Johnsrude IS, Ashburner J, Henson RN, Friston KJ, et al. (2001) A voxel-based morphometric study of ageing in 465 normal adult human brains. Neuroimage 14: 21–36.
22. Hosoi R, Matsuyama Y, Hirose S, Koyama Y, Matsuda T, et al. (2009) Characterization of (14)C-acetate uptake in cultured rat astrocytes. Brain Res 1253: 69–73.
23. Kato H, Shimosegawa E, Isohashi K, Kimura N, Kazui H, et al. (2012) Distribution of cortical benzodiazepine receptor binding in right-handed healthy humans: a voxel-based statistical analysis of iodine 123 iomazenil SPECT with partial volume correction. AJNR Am J Neuroradiol 33: 1458–1463.
24. Brownell B, Hughes JT (1962) The distribution of plaques in the cerebrum in multiple sclerosis. J Neurol Neurosurg Psychiatry 25: 315–320.
25. Chard DT, Griffin CM, McLean MA, Kapeller P, Kapoor R, et al. (2002) Brain metabolite changes in cortical grey and normal-appearing white matter in clinically early relapsing-remitting multiple sclerosis. Brain 125: 2342–2352.
26. Srivastava R, Aslam M, Kalluri SR, Schirmer L, Buck D, et al. (2012) Potassium channel KIR4.1 as an immune target in multiple sclerosis. N Engl J Med 367: 115–123.
27. Wyss MT, Weber B, Treyer V, Heer S, Pellerin L, et al. (2009) Stimulation-induced increases of astrocytic oxidative metabolism in rats and humans investigated with 1-11C-acetate. J Cereb Blood Flow Metab 29: 44–56.
28. De Keyser J, Steen C, Mostert JP, Koch MW (2008) Hypoperfusion of the cerebral white matter in multiple sclerosis: possible mechanisms and pathophysiological significance. J Cereb Blood Flow Metab 28: 1645–1651.
29. Dineen RA, Vilisaar J, Hlinka J, Bradshaw CM, Morgan PS, et al. (2009) Disconnection as a mechanism for cognitive dysfunction in multiple sclerosis. Brain 132: 239–249.
30. Bjartmar C, Kinkel RP, Kidd G, Rudick RA, Trapp BD (2001) Axonal loss in normal-appearing white matter in a patient with acute MS. Neurology 57: 1248–1252.
31. Sharma R, Fischer MT, Bauer J, Felts PA, Smith KJ, et al. (2010) Inflammation induced by innate immunity in the central nervous system leads to primary

astrocyte dysfunction followed by demyelination. Acta Neuropathol 120: 223–236.
32. Choi JW, Gardell SE, Herr DR, Rivera R, Lee CW, et al. (2011) FTY720 (fingolimod) efficacy in an animal model of multiple sclerosis requires astrocyte sphingosine 1-phosphate receptor 1 (S1P1) modulation. Proc Natl Acad Sci U S A 108: 751–756.
33. Naismith RT, Xu J, Tutlam NT, Scully PT, Trinkaus K, et al. (2010) Increased diffusivity in acute multiple sclerosis lesions predicts risk of black hole. Neurology 74: 1694–1701.
34. Sahraian MA, Radue EW, Haller S, Kappos L (2010) Black holes in multiple sclerosis: definition, evolution, and clinical correlations. Acta Neurol Scand 122: 1–8.
35. Blinkenberg M, Rune K, Jensen CV, Ravnborg M, Kyllingsbaek S, et al. (2000) Cortical cerebral metabolism correlates with MRI lesion load and cognitive dysfunction in MS. Neurology 54: 558–564.
36. Vercellino M, Merola A, Piacentino C, Votta B, Capello E, et al. (2007) Altered glutamate reuptake in relapsing-remitting and secondary progressive multiple sclerosis cortex: correlation with microglia infiltration, demyelination, and neuronal and synaptic damage. J Neuropathol Exp Neurol 66: 732–739.
37. Hyder F, Patel AB, Gjedde A, Rothman DL, Behar KL, et al. (2006) Neuronal-glial glucose oxidation and glutamatergic-GABAergic function. J Cereb Blood Flow Metab 26: 865–877.
38. Wang D, Ayers MM, Catmull DV, Hazelwood LJ, Bernard CC, et al. (2005) Astrocyte-associated axonal damage in pre-onset stages of experimental autoimmune encephalomyelitis. Glia 51: 235–240.
39. Van den Berg CJ, Mela P, Waelsch H (1966) On the contribution of the tricarboxylic acid cycle to the synthesis of glutamate, glutamine and aspartate in brain. Biochem Biophys Res Commun 23: 479–484.
40. Wyss MT, Magistretti PJ, Buck A, Weber B (2011) Labeled acetate as a marker of astrocytic metabolism. J Cereb Blood Flow Metab 31: 1668–1674.